Design and Applications of the Integrating Nephelometer: A Review

JOST HEINTZENBERG

Institute for Tropospheric Research, Leipzig, Germany

ROBERT J. CHARLSON

University of Washington, Seattle, Washington

(Manuscript received 20 October 1995, in final form 17 January 1996)

ABSTRACT

The purpose of this paper is to document the key literature references and to describe the design philosophy, the principles of the instrument, the various possible designs, calibration, systematic errors, applications to scientific problems and inherent limitations. According to the design philosophy established in the original publication, instruments are devised to directly measure the relevant integral aerosol parameters, thus eliminating the need for assumptions about particle size distribution, particle shape and composition, complex Mie calculations, and the unknown uncertainties associated with them. The key parameter measured by the integrating nephelometer is the scattering component of extinction as a function of wavelength. This philosophy subsequently allows two approaches to the determination of several parameters—direct measurement with the aid of the integrating nephelometer and calculation via the Mie formalism. Comparison of calculated and measured values for a parameter allows *closure* studies; that is, the difference between them is an objective measure of the uncertainty that is inherent in the combined set of measured and calculated parameter values.

1. Introduction

Fifty years have passed since F/Lt. R. G. Beuttell and A. W. Brewer devised geometries for and built the first *integrating nephelometers.* These instruments produce a signal that is closely proportional to the cosine weighted scattering function; the quantity needed for determination of the scattering part of the extinction coefficient. (Basic definitions of scattering properties will be provided in section 2.) The original application of the integrating nephelometer was for estimating the horizontal visibility at night, a requirement for wartime military operations. Since that time, aided in particular by development of electronic means for measuring light intensity at extremely low levels, numerous other applications of the integrating nephelometer have been found. Most recently, studies of the optical scattering efficiency of the individual chemical constituents of atmospheric aerosols have been used extensively to estimate the direct influence of aerosols on climate. Because of this long, varied and fruitful history, because there have been no reviews to document the progress of this technical development, and because of the widespread use of the integrating nephelometer, we have assembled this review. The purposes of this paper are to describe the design philosophy, the principles of the instrument, the various possible designs, calibration, systematic errors, applications to scientific problems, and inherent limitations. A companion paper (Anderson et al. 1996) includes the results of a laboratory study of the performance and calibration with both gases and monodisperse aerosols. Beuttell was killed in the early 1940s while on a meteorological reconnaissance flight, and Brewer (who had kept in close touch with Beuttell during his military service) published the designs posthumously.

2. Basic definitions of scattering properties

In this section we will introduce a number of optical properties that we shall use in subsequent discussions of nephelometer measurements. When a monochromatic parallel beam of radiation of wavelength λ with initial intensity I_0^λ, passes through a thin layer of a homogeneous aerosol, part of the radiation will be absorbed in the layer and part of it will be scattered in all directions about the initial direction of the beam. After the passage along a path of length x through the aerosol, the initial beam will be attenuated to intensity I_x^λ according to the Lambert–Beer law

$$I_x^\lambda = I_0^\lambda \exp[-(\sigma_a^\lambda + \sigma_s^\lambda)x], \qquad (2.1)$$

where σ_a^λ and σ_s^λ are the monochromatic volumetric coefficients of absorption and scattering, respectively.

Corresponding author address: Dr. Jost Heintzenberg, Institut für Troposphärenforschung e.V., Permoserstr 15, Leipzig 04303, Germany.

The sum of the two attenuation processes describes extinction, with its corresponding coefficient being σ_e^λ. Each of the coefficients has a component due to the carrier gas (index R for Rayleigh, standing for scattering and absorption of air molecules) and one due to the suspended particles (index p):

$$\sigma_a^\lambda = \sigma_{aR}^\lambda + \sigma_{ap}^\lambda \tag{2.2a}$$

and

$$\sigma_s^\lambda = \sigma_{sR}^\lambda + \sigma_{sp}^\lambda. \tag{2.2b}$$

The scattering coefficient σ_s^λ can also be defined with the help of the scattering function $f^\lambda(\Omega)$, which gives the intensity scattered in any increment of solid angle Ω about the initial direction of the beam. The integral of $f^\lambda(\Omega)$ over all directions equals the scattering coefficient,

$$\sigma_s^\lambda = \int_{\Omega=4\pi} f^\lambda(\Omega) d\Omega. \tag{2.2c}$$

In polar coordinates Φ and Θ, where Φ and Θ are the azimuthal and scattering angles, respectively, and assuming symmetrical scattering processes with respect to Φ,

$$\sigma_s^\lambda = 2\pi \int_{\theta=0}^{\theta=180} f^\lambda(\theta) \sin\theta d\theta. \tag{2.3}$$

Figure 1 illustrates the geometry of scattering and defines Θ and Φ. As with the integral coefficients [cf. Eq. (2.2b)], the scattering function $f^\lambda(\Theta)$ of an aerosol has a component from the carrier gas and one from the suspended particles

$$f^\lambda(\theta) = f_R^\lambda(\theta) + f_P^\lambda(\theta). \tag{2.4}$$

When integrating over forward and backward hemispheres, we can define the integrals over part of the scattering sphere, σ_{fs}^λ and σ_{bs}^λ, as

$$\sigma_{fs}^\lambda = 2\pi \int_{\theta=0}^{\theta=90} f^\lambda(\theta) \sin\theta d\theta, \tag{2.5a}$$

$$\sigma_{bs}^\lambda = 2\pi \int_{\theta=90}^{\theta=180} f^\lambda(\theta) \sin\theta. \tag{2.5b}$$

The ratios $\sigma_{fs}^\lambda/\sigma_s^\lambda$ and $\sigma_{bs}^\lambda/\sigma_s^\lambda$ give the fractions of the total scattered energy that is scattered per volume into forward and backward hemispheres, respectively. For a given volume, the scattering function-weighted average cosine $\overline{\cos\Theta}^\lambda$ or asymmetry factor g^λ is a measure of the angular region into which most of the scattered energy is scattered [cf. Eq. (2.6)]:

$$\overline{\cos\theta}^\lambda = \frac{2\pi}{\sigma_s^\lambda} \int_{\theta=0}^{\theta=180} f^\lambda(\theta) \sin\theta \cos\theta d\theta. \tag{2.6}$$

The ratios $\sigma_{fs}^\lambda/\sigma_s^\lambda$ and $\sigma_{bs}^\lambda/\sigma_s^\lambda$ or $\overline{\cos\Theta}^\lambda$ are used in radiative transfer calculations to take into account the angular distribution of the scattered radiation when the complete scattering function is not available or would require too large computational resources.

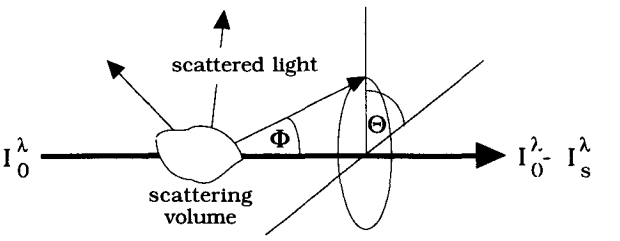

FIG. 1. The geometry of scattering. The scattering angle Θ is measured between the transmitted beam and the scattered ray. After the passage of the scattering volume, the initial intensity I_0^λ has decreased to I_s^λ.

Another quantity used in radiative transfer calculations is the single scattering albedo of the aerosol particles ω^λ:

$$\omega_p^\lambda = \frac{\sigma_{sp}^\lambda}{\sigma_{sp}^\lambda + \sigma_{ap}^\lambda} = \frac{\sigma_{sp}^\lambda}{\sigma_{ep}^\lambda} = 1 - \frac{\sigma_{ap}^\lambda}{\sigma_{ep}^\lambda}. \tag{2.7}$$

Koschmieder (1924) formulated a theory that relates σ_e^λ to the horizontal visual range through the atmosphere. For a contrast threshold of the observer of 2% and for the wavelength of maximum photopic sensitivity of the eye, the meteorological visibility or visual range V_N can be defined with the help of Koschmieder's theory as

$$V_N = \frac{3.9}{\sigma_e^{\lambda=0.55\,\mu m}}, \tag{2.8a}$$

or with the scattering coefficient

$$V_N = \frac{3.9}{\sigma_s^\lambda}\left(1 - \frac{\sigma_a^\lambda}{\sigma_e^\lambda}\right) = \frac{3.9}{\sigma_s^\lambda}\omega^\lambda, \quad \lambda = 0.55\,\mu m. \tag{2.8b}$$

The correct spectral weighting of V_N was discussed by Ruppersberg (1978). Except for the cases of highly absorbing smoke and pollution situations, the absorption factor $\sigma_a^\lambda/\sigma_e^\lambda$ has values of 0.3 or smaller. Thus, V_N can be determined approximately from the scattering coefficient at $\lambda = 0.55\ \mu m$.

$$V_N \approx \frac{3.9}{\sigma_s^\lambda}, \quad \text{for} \quad \frac{\sigma_a^\lambda}{\sigma_e^\lambda} \ll 1, \quad \lambda = 0.55\,\mu m. \tag{2.8c}$$

In the atmosphere, the scattering coefficient σ_s^λ is the sum of the Rayleigh scattering coefficient σ_{sR}^λ and the particle scattering coefficient σ_{sp}^λ. There are analytical formulas and empirical results for calculating σ_{sR}^λ for air and other gases (Kasten 1968; Bhardwaja et al. 1973; Cutten 1974; Bodhaine 1979). For arbitrarily shaped or inhomogeneous scattering objects that are of sizes that are on the same order of magnitude as the wavelength or larger, there is no general theory relating the physical parameters of the object and its scattering

behavior. Because of the polydisperse nature of the atmospheric aerosol, the size distribution—for example, the number concentration of the scatterers as a function of their size—is an essential determinant for atmospheric scattering processes. Besides the size distribution, particle shape, and complex index of refraction m^λ affect angular and integral scattering of radiation;

$$m^\lambda = n^\lambda - ik^\lambda,$$

with n^λ being the real part and k^λ being the imaginary part ($i = \sqrt{-1}$). For homogeneous, symmetrical scatterers, a theory developed by Mie (1908) and formulated for the atmospheric aerosol by van de Hulst (1957) and others, allows the calculation of the scattering properties of a polydisperse particle population from the knowledge of size distribution and refractive index.

3. Instrument designs to yield desired integrals

a. Beuttell and Brewer's optical designs

Faced with a need to measure the extinction of light in the atmosphere, it might seem appropriate to measure I_0^λ and I^λ after transmission through a distance x; after all, measurement of extinction is an age-old practice in the laboratory, for example, in spectrophotometers. However, the atmosphere immediately imposes a severe problem due to the typical small magnitude of σ_e^λ (i.e., $\sigma_a^\lambda + \sigma_s^\lambda$). Values of σ_e in clean air for visible light typically are around 10^{-5} m^{-1}, polluted air has roughly $10^{-4} \leq \sigma_e^\lambda \leq 10^{-3}$ m^{-1}, and fogs range around $10^{-2} \leq \sigma_e^\lambda \leq 10^{-1}$ m^{-1}. Thus, unless the fog is thick, it is necessary by Eq. (2.1) to have $x > 100$ m in order to have I^λ/I_0^λ be much smaller than one, which is required for accuracy of determining σ_e^λ. Having $x > 100$ m (let alone having $x > 10^5$ m for clean air) is inconvenient and, importantly, σ_e^λ varies extensively over such distances. Further, measuring σ_e^λ may satisfy some applications, but (as will be seen in sections 8–10) having separate measures of σ_s^λ and σ_a^λ is important, especially when considering the connections between chemical composition and optical extinction or the climatic forcing due to aerosol.

Beuttell developed a series of instrument designs that obviated the problems of transmissiometry by integrating the scattering function [Eq. (2.3)]. One obvious way to perform this integration was to measure $f^\lambda(\Theta)$ with a polar nephelometer—that is, measure scattered intensity as a function of Θ, as is done with a goniometer. While this had already been achieved by Waldram (1945), polar nephelometers are clumsy to operate, require substantial postmeasurement manipulation of data, and do not always have adequate sensitivity. Today, this could be accomplished easily with modern computers (Jones et al. 1994), but such was not the case in the early 1940s, leading Beuttell to devise optical geometries that perform the desired integration. Two basically different approaches correctly integrate the polar curve of scattering; the reader is referred to the companion paper for a formal derivation (Anderson et al. 1996).

1) A parallel light beam and a detector mounted as shown in Fig. 2, which views light scattered over most of the range from $0 \leq \Theta < \pi$. If the sensitivity of the detector is independent of the direction of illumination, a weighting of $\cos(90° - \Theta)$ exists due to the geometry. Because the detector is aligned at 90° to the optical axis since $\cos(90° - \Theta) = \sin\Theta$, the weighting desired for Eq. (2.3) is attained. Beuttell used a 100-W lamp, a collimating lens, and a selenium barrier cell connected to a recorder to provide a continuous record of σ_s, obviously integrated over a wide wavelength range.

2) A cosine law, diffuse light source, and a detector arranged to view a volume, with each increment of scattering angle being weighted equally. There actually are three versions of this geometry: (i) a conical viewing volume, (ii) a columnar volume, the light from which is collected by a lens, and (iii) an integrating volume, the interior of which is reflective so as to provide an omnidirectional light flux, coupled to a focused sensing volume. Figure 3 illustrates the fundamental components of these three geometries with diffuse illumination. All three of these have the sensing or viewing volume located in front of a blackened light trap such that zero intensity would correspond to $\sigma_s = 0$. Owing to the small scattered light intensities that are available with these three similar geometries, a selenium photocell of the 1940s was insufficient and the human eye became the sensor. Clever optical arrangements were designed for simultaneous viewing of scattered light and light from the source viewed through a gray wedge, with empirical calibration, for example, at known V_N.

All of these geometries suffered due to truncation of the scattering volume near $\Theta = 0$ and $\Theta = \pi$. All of them also used a broad wavelength band, which was much too broad for most current applications. Sensitivities were not very great, and the instruments were chiefly used in fog, with $V_N \approx 1$ km or less. Calibration using known V_N undoubtedly introduced large errors, for example, due to spatial inhomogeneity of σ_s. The best results were apparently obtained with a cosine light source and when the instrument was used as a nighttime

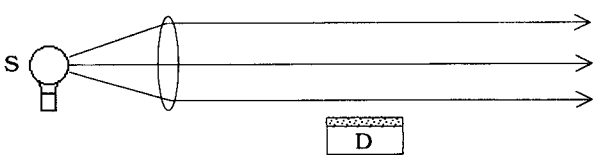

FIG. 2. Integrating nephelometer geometry with columnar illumination and wide angle detection: *S*—light source, *D*—detector with cosine-law diffuser.

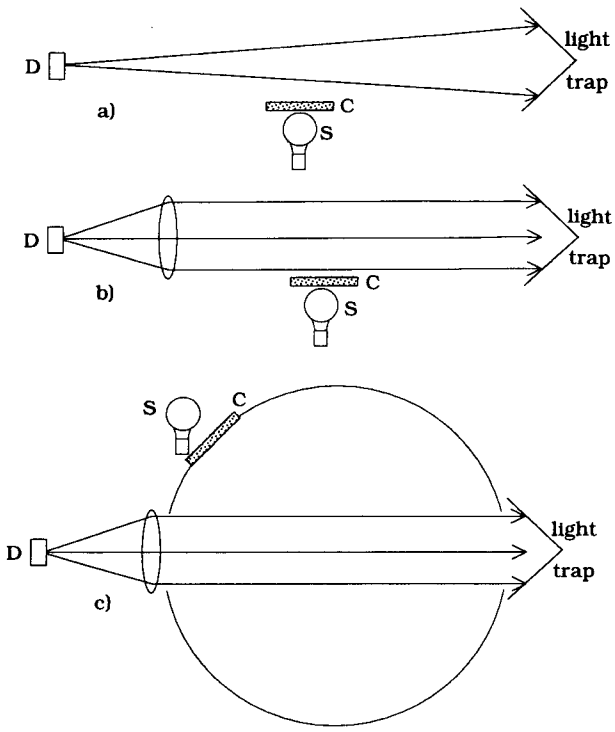

FIG. 3. Integrating nephelometer geometry with cosine-law illumination and narrow angle detection: S—light source with (a),(b) cosine-law diffuser and (c) an additional integrating sphere, D—detector.

visibility meter. Improvements beyond the capabilities of these crude, manually operated devices required the development of much improved photosensors, geometries that were more refined and characterized, narrow wavelength bands and, perhaps most importantly, means for absolute and accurate calibration.

b. Extensions of the designs

The original optical designs given by Beuttell have been realized in different ways, and most have used one or another of the second kind of integrating geometry (wide-angle illumination and narrow angle detection). Following Beuttell's idea of employing the scattering coefficient as a measure of visibility, Ruppersberg built an open chamber nephelometer with flash-lamp light source in the 1950s (Ruppersberg 1959), with the first refereed report being Ruppersberg (1964). The instrument integrated over an angular range of roughly 20°–120°. Because of its use for unattended long-term operation on lighthouses, airport runways, and highways, the electronics were based on an extremely stable zero-compensation principle (as was employed manually in the original Beuttell design). The spectral sensitivity of the instrument was adjusted to the photopic state of the human eye. Expressed in visibilities V_N, the dynamic range of the original instrument was 40 m to 40 km. Later, the spectral range of the instrument was extended for atmospheric aerosol studies, first by building a separate unit operating near the wavelength of peak emission of the flash lamp ($\approx$0.85 μm) (Heinicke 1967; Ruppersberg et al. 1972) then by filtering both sample and reference light path with six filters between 0.43- and 0.920-μm central wavelength (Heintzenberg 1969). By using a silicon detector instead of vacuum photodiodes in these later research-type instruments, the dynamic range could be extended to about 200 km.

Beuttell's second design was employed first in an open chamber design by Crosby and Koerber (1963) that integrated over the angular range of roughly 10°–165°. The same design was used in the first closed chamber nephelometer by Ahlquist and Charlson (1967). Integrating from 7° to 172° with an opal glass in front of a xenon flash lamp, the cosine characteristic of the angular illumination was closely realized. The disadvantage of affecting the thermodynamic state of the aerosol by sampling it through a warm chamber was offset by the possibility of calibrating the instrument with Rayleigh scatterers with known scattering properties (e.g., chlorofluorocarbons or CO_2, cf. section 4). With the closed chamber approach, very low levels of stray light existed so that photomultiplier tubes could be used as detectors. This greatly enhanced the sensitivity of the instrument to the extent of being able to measure the scattering coefficient of air ($\sigma_{sR}^{\lambda=0.55\ \mu m} \approx 10^{-5}$ m^{-1} at STP). Consequently, the Rayleigh scattering component of the signal could be subtracted during the measurement allowing the direct output of the aerosol scattering coefficient.

A similar angular range was realized in a partly closed nephelometer for visibility studies developed by Garland and Rae (1970). Their open design was optimized for atmospheric visibility studies. Because of that, the calibration of the instrument was as problematic as with the Ruppersberg design (cf. section 4).

As with the Ruppersberg instrument, the spectral range of this sensor also was extended. The first construction of a multiwavelength unit is described by Ahlquist and Charlson (1969). The widest spectral range for this type of design, ($0.45 \leq \lambda \leq 0.875$ μm), was realized in the unit used by Heintzenberg (1975) in order to maximize the information content with respect to particle size distribution (cf. section 6). By adding a Czerny–Turner-type spectrometer in front of the detector, Harrison (1977) derived continuous spectra of σ_{sp}^{λ} in the visible and near infrared. No detection limits were given by the author.

Eventually, the initial flash lamp was replaced by a continuous quartz-halogen incandescent lamp and the scattered light was measured by photon counting techniques, again using photomultiplier tubes (Charlson et al. 1974). Further design improvements included an additional chopper that allowed the separate measurement of (a) attenuated direct light from the opal glass

and (b) the dark counts of the detector. Automated calibrations with filtered air were complemented by temperature and pressure measurements in the chamber in order to subtract the density-dependent instantaneous Rayleigh scattering component in between air calibrations (Heintzenberg and Bäcklin 1983). These additional signals, together with electronic improvements and online data processing in an internal microcomputer allowed detection limits down to 10^{-8} m^{-1} for σ_{sp}^{λ} and airborne operations with 1-Hz time resolution up to 12-km altitude (Heintzenberg et al. 1991; Bodhaine et al. 1991).

The only realization of Beuttell's third wide-angle illumination design (omnidirectional illumination with narrow angle detection) was reported by Gerber (1986). In this closed chamber nephelometer, the omnidirectional illumination of the aerosol is achieved by designing the scattering chamber in the form of an integrating sphere that is illuminated by a flash lamp through an opening. Gerber's lightweight, balloon-borne instrument had an angular scattering range of 5°–173° and detection limit of about 0.4×10^{-5} m^{-1} at 1-s time constant for $\sigma_{sp}^{\lambda=0.55\ \mu m}$. Beuttell's first design (columnar illumination and wide-angle detection) has been used rarely. For example, Nyeki et al. (1992) reported a novel combination of an integrating nephelometer with a cascade impactor to yield size-resolved information on σ_s.

4. Calibration approaches

The calibration of the original integrating nephelometer constructed by Beuttell depended on comparisons of the instrument reading with observations of the ambient visual range, complemented by the use of two diffusely scattering disks to scatter a known fraction of the light source output toward the observer (detector). Also, later designs of open chamber integrating nephelometers employed diffuse scatterers of either a reflective type, (Crosby and Koerber 1963; Garland and Rae 1970) or a transmission type (Ruppersberg 1964). The angular scattering characteristics of these calibration devices had to be measured for the specific arrangement of the respective integrating nephelometer (Heinicke 1967; Heintzenberg 1969). With the aid of linearity experiments, a calibration curve was extrapolated over the entire dynamic range (two to three orders of magnitude) of the instruments from this single calibration point with a relative uncertainty of roughly 5%.

The advent of the integrating nephelometer with a closed scattering volume allowed the use of gases with known scattering properties for the calibration of integrating nephelometers (Charlson et al. 1967; Bhardwaja et al. 1973). Such Rayleigh scatterers have scattering functions and wavelength dependence that differ strongly from those for typical atmospheric aerosols. Thus, the difference in angular and spectral response between calibration gas and the aerosol had to be taken into account when deriving aerosol scattering coefficients. By using different gases, a calibration range of several orders of magnitude could be covered. Helium, scattering only about 1% as much as air, yielded an estimate of the background signal of the instrument without scatterers in the sensing chamber. An easier way of assessing the background signals of vacuum-tight integrating nephelometers was possible with later instrument designs that allowed evacuation of the sensing chamber (Heintzenberg and Bäcklin 1983). This design also provided the possibility of determining a gas calibration curve of the instrument with particle-free air by simply changing the density during the calibration.

In principle, the most appropriate calibration of the integrating nephelometer would be achieved with known particles approximating the ambient aerosol. Keeping in mind the different particle properties that affect their scattering characteristics and the technical difficulties in controlling them, this type of calibration poses a difficult task. First attempts at such a calibration by Heintzenberg (1975) were limited by the state of techniques in generating and characterizing calibration particles, but took into account the specific truncation error for the latex aerosol calculated by Heintzenberg and Quenzel (1973a). With these data, it was possible to reconcile the manufacturer's information on submicrometer polystyrene latex particles, their multiwavelength signals in an integrating nephelometer, and readings from an optical particle counter within the range of experimental uncertainties (≈20%). A companion paper reports on recent experiments comparing gas and aerosol calibrations of the integrating nephelometer (Anderson et al. 1996).

5. Accuracy of the angular integration

Initially, the integrating nephelometer was developed as an instrument for the determination of the visual range, assuming the approximate relationship of Eq. (2.7c), and measuring $\sigma_{sp}^{\lambda=0.55\ \mu m}$. The optical construction of the integrating nephelometer, (cf. section 3) causes a systematic error due to the truncated angular range of optical integration. Considering the various individual designs, the first 8°–20° of scattering angle and the last 8°–60° are excluded from the measurement. In the original publication (Beuttell and Brewer 1949), this error was considered to be negligible because of the small solid angle included in the forward and backward regions. However, for scatterers larger than the wavelength, much of the scattering is in the forward direction such that this truncation error becomes dependent on the size of the scattering particles. In recognition of this problem, Mie scattering calculations have been done for several of the different instrument geometries and for different types of scattering particles (Quenzel 1969; Ensor and Waggoner 1970; Heintzenberg and Quenzel 1973a; Quenzel et al. 1974; Rabinoff and Herman 1973; Quenzel et al. 1975; Har-

rison 1979; Marshall 1994). Truncation errors on the order of 10%–20% were found in these calculations for size distributions like that of the atmospheric aerosol. Most of these truncation studies were limited by the assumption of idealized angular characteristics of the instruments. To date, the angular characteristics of only two nephelometers have actually been directly measured for their use in truncation estimates (Heinicke 1967; Heintzenberg 1978), while (Marshall 1994) did consider the nonideality of the light source; truncation angle and backscatter shutter. Because of nonideal source characteristics and reflections from the nephelometer optics, they all found significant deviations from the idealized sinusoidal weighting of the angular response.

Since there is a systematic shift in scattered light with increasing particle size toward smaller scattering angles, the largest particle size observable with a truncated nephelometer has been calculated for fixed relative errors of the instrument (Heintzenberg and Quenzel 1973b). They found that particles larger than 4 μm in an aerosol with a power-law size distribution with $\nu^* = 2$–4 (cf. section 7) do not contribute significantly to measurements with the Ahlquist–Charlson type nephelometer.

The accuracy of the σ_{bsp}^{λ} measurement was investigated theoretically by Heintzenberg and Bhardwaja (1976) who found a range −3% to +5% for the angular truncation error for σ_{bsp}^{λ}. Because of the additional optical element of the backscatter shutter in the modified instrument, their results pointed to the need for a calibration of the angular characteristics of the modified integrating nephelometer. In a later study, this quantity was determined for the integrating nephelometer that was used in the early backscatter studies (Heintzenberg 1978).

6. Studies of visual range and/or path transmittance

The need for measurement of visual range or path transmittance is based on both practical and aesthetic considerations. Practical issues such as the visual range at airports or transmission of military laser beams are obvious examples. The main aesthetic concern is the appearance of haze and subsequent degradation of scenic vistas. In either case, significant problems exist due to the difficulties posed by the need for information over long pathlengths. Measurements that are made at a point or over pathlengths that are short compared to the visual range may not be representative of the whole path. Even so, it is usually necessary to use local, point measurements due to the practical and logistical difficulty of deploying optical instruments over paths of 10–100 km or more.

If one of the goals of determining visual range is to identify and characterize the aerosol that influences or degrades visibility, then optical measurements made at a point are even more necessary because aerosol characterization instruments and samplers also operate at a point. It is true that both types of instruments collocated in aircraft can provide data along a light-and-sight path; however, the cost of doing this usually is much too large. In any case, time-averaged optical data acquired at a point often correlate quite well with long-path observations even though the aerosol may not always be well mixed on spatial scales of tens of kilometers.

Data acquired simultaneously with the integrating nephelometer and visibility observations bear out the reality of this suggestion. While only a few studies have been published, they provide tests of the Koschmieder theory, (Koschmieder 1924) (cf. Horvath and Noll 1969; Dzubay et al. 1982). High (0.8–0.9) correlation coefficients were determined between $\sigma_{sp}^{\lambda=0.5\ \mu m}$ and the reciprocal of visual range observations at RH < 60%. Comparison to Koschmieder theory further suggests that $\sigma_{ap} < \sigma_{sp}$. Numerous papers exist on measurement of σ_s for studies of visibility, as summarized in Trijonis et al. (1990).

Because closed-chamber integrating nephelometers do heat the sample air, the measured scattering coefficient will be decreased if a significant amount of water exists within the aerosol particles. However, Beuttell and Brewer (1949) pointed out that the low RH measurement indicates the portion of the scattering due to the aerosol itself, which is an important quantity (cf. section 9).

7. Spectral scattering studies related to size distribution and refractive index

Early spectral extinction measurements in the atmosphere suggested a connection between the size distribution of the attenuating particles and the shape of the extinction spectrum (Ångström 1929). In the visible region this spectrum often could be approximated by a power law whose exponent $\mathring{a}$ has been termed Ångström exponent:

$$\sigma_{ep}^{\lambda} \propto \lambda^{-\mathring{a}}. \tag{7.1}$$

Junge (1952) developed a model for the number size distribution $dn/d\log r$ of the atmospheric aerosol where he related particle radius r and concentration through a power law with the exponent ν^*. He found the analytical relationship

$$\mathring{a} = \nu^* - 2, \quad \text{where} \quad \frac{dn}{d\log r} = \text{const} \times r^{-\nu^*} \tag{7.2}$$

between the exponents of the two power-law approximations for the extinction spectrum and size distribution, respectively. Despite the inherent limitations in the two power-law approximations, the relationship (7.1) has been used ever since to interpret spectral extinction measurements in the visible spectrum in terms

of the shape of the underlying size distribution of attenuating particles.

When direct measurements of σ_{sp}^{λ} became feasible (Ahlquist and Charlson 1969; Heintzenberg 1969), this approach was extended to spectral scattering measurements as well. Thus, integrating nephelometer spectra were interpreted in terms of the size distribution of particles in the scattering chamber. This extension required the additional assumption that the absorption part of the extinction does not affect the relationship (7.1) when applying it to the scattering component of the spectral extinction.

The first efforts to retrieve the underlying size distribution from integrating nephelometer spectra in the visible and near-infrared region without the constraints of both power law assumptions were reported by Heintzenberg (1975). He found that the data from the integrating nephelometer had to be complemented by information from other aerosol sensors in order to retrieve realistic size distributions in the accumulation range ($0.05 \leq r \leq 0.5$ μm). Realizing the limited information content of nephelometer derived spectra, Heintzenberg (1977) derived an optically effective particle radius. Later, the approach of combining data from a single wavelength integrating nephelometer with those from other aerosol instruments has been used by Sverdrup and Whitby (1977) to derive particle size distributions.

Harrison (1977) used continuous spectra of σ_{sp}^{λ} for $0.35 \leq \lambda \leq 0.75$ μm to estimate the size distribution of atmospheric particles in the diameter range 0.14–3 μm. In these first attempts to derive size distributions from nephelometer data (Heintzenberg 1975), and in later studies backscatter information Heintzenberg (1980), reconciling nephelometer information with that from other particle sensors required the interpretation of the nephelometer data as spectral integrals over the scattering function weighed with the angular characteristics of the particular instrument. With that approach the influence of the systematic truncation error could be minimized. The size information of σ_{sp}^{λ} for $0.45 \leq \lambda \leq 0.9$ μm has been investigated by Heintzenberg (1985) without any inherent assumptions about the shape of the underlying particle size distribution.

In early models of the influence of the atmospheric aerosol on climate, the backscatter ratio $\sigma_{bsp}^{\lambda}/\sigma_{sp}^{\lambda}$ was used to describe the cooling effect of the aerosol (Sagan and Pollack 1967; Wiscombe and Grams 1976). By a modification of the integrating nephelometer design, this quantity could be measured directly by the instrument (Charlson et al. 1974). For typical atmospheric aerosol size distributions, it was soon discovered that this ratio is strongly dependent on the real part n^{λ} of the refractive index of the scattering particles. Consequently, this effect was utilized to derive estimates of the refractive index of atmospheric aerosol (Bhardwaja et al. 1974; Bhardwaja et al. 1976). In the case of nonabsorbing aerosols and mid-visible wavelength, the accuracy for refractive index was estimated to be $|\Delta n^{\lambda}| \approx 0.05$, while being about 0.1 for moderately absorbing particles. Unfortunately, the magnitude of this uncertainty precludes using the backscatter/total scatter ratio for inference of chemical composition.

Mathai and Harrison (1980) took yet another route to derive an estimate of the real part of the refractive index n^{λ}. Their input data were parallel measurements with a single wavelength nephelometer of the Ahlquist–Charlson type and an optical particle counter. Assuming a power-law size distribution, they derived an estimate of the refractive index from look-up tables of $\sigma_{sp}^{\lambda=0.48\ \mu m}$ calculated with Mie-theory for power-law size distributions with different exponents and different values of n^{λ}. This approach has not yet been extended to more modern representations of the size distribution.

The feasibility of extending the spectral range of the integrating nephelometer into the ultraviolet region has been demonstrated by Heintzenberg and Witt (1979). They were able to measure σ_{sp} down to $\lambda = 0.25$ μm. Consequently, information on smaller particles than with conventional integrating nephelometers could be derived from this extended wavelength range.

8. Studies of mass scattering efficiency α_M

Prior to 1967, there was a widely held belief that the aerosol size distribution was so variable and (in particular) that the abundance of supermicrometer sized particles was a major factor, such that a unique relationship of σ_e^{λ} or visual range to any measure of mass concentration would never be found. At that time (as noted above) the size distribution was often described by a power law with the exponent ν^* varying from roughly 2.5 to 4. Calculations showed that the scattering efficiency would be expected to be strongly influenced by the large-particle cutoff of the power-law function. However, up to the late 1960s, there were only indirect means to estimate σ_e^{λ} (via visual range or optical depth); visibility was thought to be mainly controlled by humidity (RH), and only crude methods were available for evaluating mass concentration; the net result was a lack of definitive conclusions.

The advent of the closed-chamber integrating nephelometer in 1966 allowed the determination of σ_{sp}^{λ} on one-and-the-same air sample as the mass content, and allowed the control of RH as well. Inasmuch as filter samples for mass determination normally were (and still are) desiccated prior to weighing, it was decided to heat the integrating nephelometer by roughly 10°C to reduce RH to less than roughly 50%. Charlson et al. (1968) reported a high linear correlation coefficient ($\approx$0.9) between σ_{sp}^{λ} and gravimetrically determined mass concentration with a regression slope of close to 3 $m^2\ g^{-1}$. The sampler for mass determination was a small (2.5 cm) membrane (Nuclepore®) filter in an open-faced, downward pointing holder configuration,

located on top of a building at roughly 70-m altitude in New York City.

Soon after this original effort, the large multivariate aerosol study in 1969 at the California Institute of Technology revealed the now widely observed and accepted bimodal volume (or mass) distribution (Husar et al. 1972). This study also revealed that the sampler used by Charlson et al. (1968) had inadvertently excluded most of the so-called coarse-mode mass above 1 μm of diameter due to the filter configuration and sampling height. Development of samplers for deliberate sampling of accumulation-mode particles with controlled cut size followed soon thereafter, as reviewed by Dzubay et al. (1982). Trijonis (1990) summarizes large amounts of data, illustrating the near-constancy of $\alpha_M^{\lambda=0.5\,\mu m}$ at 3 $m^2\ g^{-1}$ for submicrometer atmospheric aerosol. However, strict intercomparisons of various measures of α_M are not possible due to the use of different cut-sizes of samplers.

Again, using this large database acquired using the integrating nephelometer, sensitivity analyses based on Mie calculations showed that α_M is expected to be only weakly dependent either on the mass-mean size of the accumulation mode or on the refractive index of the aerosol particles (see, e.g., White 1986), and neither of these parameters varies much.

Extensions of the study of mass scattering efficiency have also included the apportionment of σ_{sp}^{λ} to the individual chemical species comprising the light scattering aerosol. If the mass concentration of a chemical species x is M_x and the total aerosol mass concentration is M, then the mass scattering efficiency of x at wavelength λ can be defined as (Anderson et al. 1994)

$$\alpha_s = \frac{\partial \sigma_{sp}}{\partial M_x} = \frac{\partial \sigma_{sp}}{\partial M}\frac{\partial M}{\partial M_x} = \alpha_M \frac{\partial M}{\partial M_x}. \qquad (8.1)$$

The earliest studies of scattering by an individual chemical species (sulfate ion) simply correlated measured σ_s with $M_{SO_4^{2-}}$, and suggested both a high efficiency ($\alpha_{SO_4^{2-}} \approx 5\ m^2\ g^{-1}$) and modestly high correlation coefficient. However, the lack of analyses of the other chemical species that had to be present, notably the cation associated with the SO_4^{2-}, prevented a proper determination of the partial derivative in Eq. (8.1). Much more thorough chemical analyses became possible in the early 1980s with the advent of ion chromatography, leading to more extensive efforts to attribute scattering to individual chemical compounds and, thence, to sources (White 1986).

9. Studies of effects of relative humidity, ammonia, and temperature on σ_{sp}

It was already widely known at the time of Beuttell and Brewer (1949) that light extinction coefficient and visibility through the atmosphere are strongly influenced by relative humidity (RH). The cause of this influence in general is the uptake of water by the aerosol particles, which causes them to grow as RH is increased. This process in turn is strongly dependent on the chemical composition of the particles, specifically on the hygroscopicity and solubility of constituents of the particles. Sufficiently soluble substances within particles exist in a dissolved form as an aqueous solution with an equilibrium concentration given approximately by Raoult's law (neglecting curvature effects and solute nonideality); where X_{H_2O} is the mole fraction of H_2O in the hydrated aerosol particle:

$$\mathrm{RH} \approx X_{H_2O} = \frac{n_{H_2O}}{n_{H_2O} + n_x}. \qquad (9.1)$$

Here n_{H_2O} and n_x are the number of moles of water and solute, respectively, within the particle. As a result, when RH approaches 100%, the amount of water in the particle grows to a large fraction of its mass and the light scattering can be greatly increased above that at low RH.

Other variable parameters besides RH also influence σ_{sp}^{λ} and have been used for studies of the chemical composition of the aerosol, often along with varying or controlling RH. Reactive gases can change the molecular form of the aerosol, for example,

$$2NH_3\ (\mathrm{gas}) + H_2SO_4\ (\mathrm{particle}) \rightarrow (NH_4)_2SO_4\ (\mathrm{particle}),$$

which can in turn change several optically important properties of the aerosol (e.g., refractive index, particle phase, shape, mass, or volume), which changes the measured value of σ_{sp}^{λ} (Heintzenberg 1978), σ_{bsp}^{λ}, and, probably, $\mathring{a}$. This application of the integrating nephelometer generally involves pretreatment of the aerosol, with measurement of σ_{sp}^{λ} being made before and after the aerosol is pretreated. Temperature also can be used in pretreatment, and is very useful for separating the amount of s_{sp}^{λ} due to refractory materials (e.g., NaCl or silicates) from volatile ones (e.g., organic condensates or any of the sulfates compositionally between H_2SO_4 and $(NH_4)_2SO_4$ (Rood et al. 1985).

Three general areas of application have been developed that use the integrating nephelometer in conjunction with control and/or measurement of RH, reactive gases, and temperature inside the closed chamber of the nephelometer; broadly termed (i) radiative transfer, (ii) cloud nucleation, and (iii) chemical inference. (In fact, the earliest version of the Ahlquist–Charlson design had a closed chamber in order to allow both definition and measurement of RH; Pilat and Charlson 1966.)

Problems broadly defined as being related to radiative transfer, including visibility, haze present around scenic vistas, transmission of solar radiation, and transmission of light from collimated or diffuse sources

through the atmosphere, require knowledge of the quantitative increase of σ_{sp}^{λ} as RH is increased. If $\sigma_{sp}^{\lambda}(\mathrm{RH})$ is the scattering coefficient at some humidity and $\sigma_{sp}^{\lambda}(0)$ is that at low or zero RH, a response function $f(\mathrm{RH})$ can be defined as

$$f(\mathrm{RH}) = \frac{\sigma_{sp}^{\lambda}(\mathrm{RH})}{\sigma_{sp}^{\lambda}(0)}. \qquad (9.2)$$

While $f(\mathrm{RH})$ can be approximated from ab initio calculations based on size distribution and chemical composition or from the measured increase in the mass of sampled aerosol particles as RH is increased (Hänel 1976; Hegg et al. 1993; Winkler 1973), σ_{sp}^{λ} can be measured while RH is measured or controlled. Figure 4 includes example data acquired with an integrating nephelometer equipped with an RH controller. The consistency of these integrating nephelometer results with the corresponding gravimetric data was checked by Winkler et al. 1981. Hygroscopic and/or soluble materials usually are present, causing roughly a 70% increase in σ_{sp}^{λ} at RH $\sim$ 80%, at least in the locations where such observations have been made (Charlson et al. 1974c; Charlson et al. 1984; Covert et al. 1980). Figure 4a shows typical σ_{sp}^{λ} versus RH data from a rural area outside St. Louis, Missouri, while Fig. 4b shows the frequency of occurrence of results at 80% RH. Measurements of $\sigma_{sp}^{\lambda}(0)$ and $f(\mathrm{RH})$ coupled with knowledge of the variation of RH over an optical path (e.g., vertical or horizontal) then can be used for comparison to long-path observations (cf. section 6).

A unique application of the integrating nephelometer was found by Radke and Hobbs (1969), in which the closed optical chamber was replaced by a closed, thermal-diffusion cloud chamber. Because droplets are activated at RH > 100% and grow at fixed supersaturations toward a monodisperse size distribution, it was possible to use the measurement of σ_{sp}^{λ} (along with a separate determination of droplet size) as a measure of the number concentration of cloud condensation nuclei.

Studies of $f(\mathrm{RH})$ also reveal information about the chemical composition of the particles, especially when the temperature also is controlled and varied. The simplest studies used the integrating nephelometer as a detector of deliquescent compounds [i.e., NaCl, $(NH_4)_2SO_4$, $(NH_4)_3(SO_4)_2$ and NH_4HSO_4] simply by measuring $f(\mathrm{RH})$ (Charlson et al. 1974b; Vanderpol et al. 1975; Weiss et al. 1977; Charlson et al. 1978). Some of these studies allowed pretreatment of the atmospheric aerosol with NH_3 gas (at low concentration) thereby converting the hygroscopic compound H_2SO_4 to the deliquescent compound $(NH_4)_2SO_4$, as is exemplified in Fig. 4a.

If the sampled air is heated prior to measuring σ_{sp}^{λ} in an integrating nephelometer, and the increase in temperature is varied, a *thermogram* results, as in Fig. 5. This technique is particularly useful for estimating the NH_4^+ to SO_4^{2-} molar ratio when the aerosol is in the compositional range between H_2SO_4 and $(NH_4)_2SO_4$ (Rood et al. 1987a).

As can be seen in Fig. 5, H_2SO_4 (where $R = 0$) volatilizes totally at approximately 125°C, while NH_4HSO_4 ($R = 1$) is the most refractory, not volatilizing until 250°C is reached. $(NH_4)_2SO_4$ shows complex behavior, with evidence of cracking at 50°C, prior to volatilization at 250°C.

It appears to be possible to use reactive gases other than NH_3 and condensible vapors other than H_2O for inference of chemical properties; however, to date, only NH_3 and H_2O have been used.

10. Future use of integrating nephelometers for estimating the asymmetry parameter

To date, the three basic geometries given by Beuttell have been realized in various designs of the integrating nephelometer, complemented in later years by wavelength resolution and the division of the angular range into backward and total scatter region. This later modification can be used as the starting point for the direct measurement of the asymmetry parameter $\overline{\cos\Theta}^{\lambda}$, defined in Eq. (2.6). In the Ahlquist–Charlson-type nephelometer, an opal glass diffuser gives the required sine-weighing of the scattering function for the optical integration of the scattering coefficient [cf. Eq. (2.3)]. Dividing the angular integration into forward and backward hemispheres yields

$$\overline{\cos\theta}^{\lambda} = \frac{2\pi}{\sigma_s^{\lambda}}\left[\int_{\theta=0}^{\theta=90} f^{\lambda}(\theta)\sin\theta\cos\theta d\theta + \int_{\theta=90}^{\theta=180} f^{\lambda}(\theta)\sin\theta\cos\theta d\theta\right],$$

which is illustrated in Fig. 6, showing how a combined sine–cosine weighting applied to the scattering function in order to integrate the signal would yield $\overline{\cos\Theta}^{\lambda}$. This weighting might be achieved by masking the opal glass in the lateral direction, that is, perpendicular to the viewing direction of the detector in a cosine shape. Such an arrangement would have a zero response at 0°, 90°, and 180°. Since the value of the integrand of $\overline{\cos\Theta}^{\lambda}$ is negative in the second quadrant, the back scatter signal of a $\overline{\cos\Theta}^{\lambda}$ nephelometer would have to be subtracted from the total scatter signal to derive the final result. The realization of this instrument would provide a means for continuously recording the asymmetry parameter, which would be useful in providing information on its temporal and spatial variability for modeling climate forcing by aerosols.

11. Applications of the integrating nephelometer to studies of climate forcing by aerosols

Besides the possibility of development of this specialized integrating nephelometer to measure the asymmetry parameter, five different applications of the in-

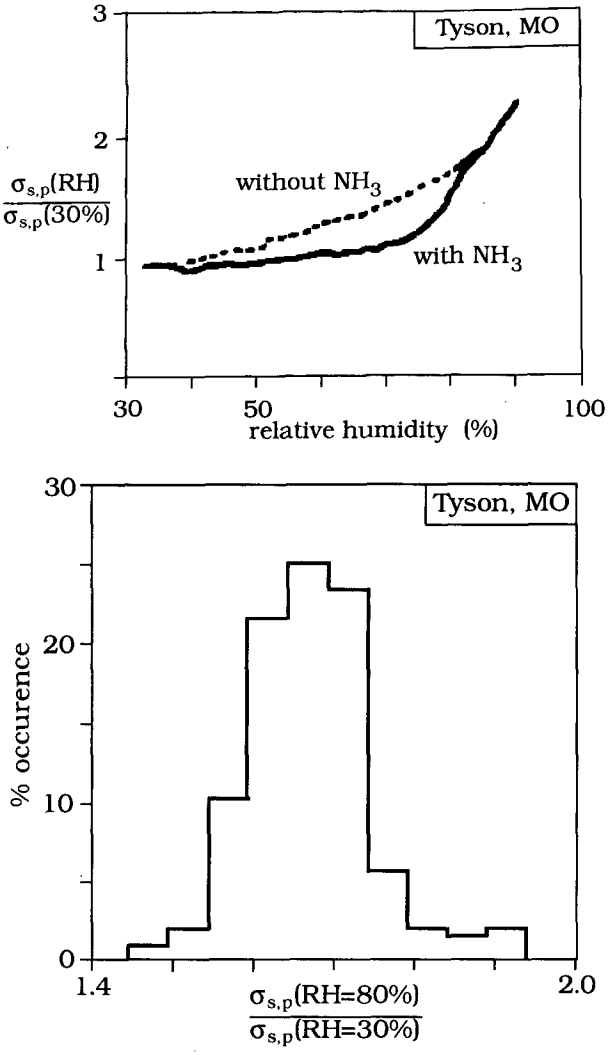

FIG. 4. (a) Example humidogram measured with an integrating nephelometer at Tyson, Missouri (cf. Charlson et al. 1978). (b) Frequency of occurrence of different scattering coefficients at a given RH of 80% at Tyson, Missouri (cf. Charlson et al. 1978).

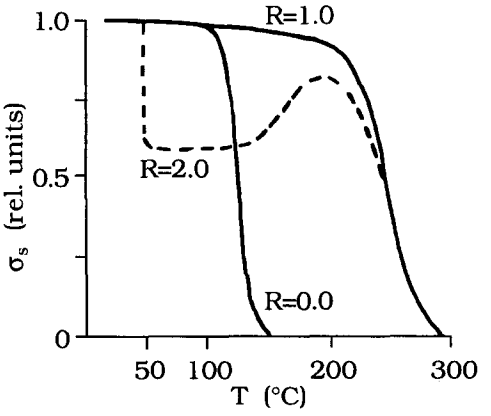

FIG. 5. Laboratory thermograms of sulfate aerosols where R is the NH_4^+ to SO_4^{2-} molar ratio between zero and two (Rood et al. 1987b). The RH of the nephelometer was held at 65%, which is below the deliquescence point of $(NH_4)_2SO_4$ but above that of NH_4HSO_4.

tegrating nephelometer are already in use for providing aerosol parameters for quantitative modeling of direct climate forcing by aerosols. *Forcing* is defined as a change in the energy balance of the earth's surface ($W\ m^{-2}$), such change being imposed in a manner that is external to the climate system itself. *Direct* forcing occurs when a perturbation of the atmospheric aerosol causes a change in the amount of solar radiation reflected by the aerosol into space, while *indirect* forcing is caused by changes in clouds or other climate related parameters due to their interactions with changes in the aerosol. Examples of aerosol changes that cause forcing are anthropogenic production of sulfate compounds from SO_2, smoke from biomass combustion, and stratospheric aerosol from large volcanic eruptions.

These five different applications of the nephelometer are discussed here.

a. Factors controlling direct climate forcing by nonabsorbing aerosols at one wavelength: The role of the integrating nephelometer

A simple algebraic expression suffices for defining the key aerosol parameters that determine direct forcing due to scattering by aerosol species x under clear skies. Equation (11.1) indicates the measurements that can be made with the integrating nephelometer in order to provide quantitative measurement of some of the key parameters. Of course, it is possible to calculate the inputs to Eq. (11.1) from assumed aerosol properties; however, the acquisition of empirical data at the very least provides quantities against which the calculated integral aerosol properties can be compared. The simplest case of clear sky, no light absorption and sun in the zenith (directly overhead) yields a reflected flux of radiation ΔF_R^λ, due to illumination at wavelength λ of S^λ:

$$\Delta F_R^\lambda = S^\lambda f^\lambda(\mathrm{RH})\beta_0^\lambda \alpha_{sx}^\lambda B_x, \qquad (11.1)$$

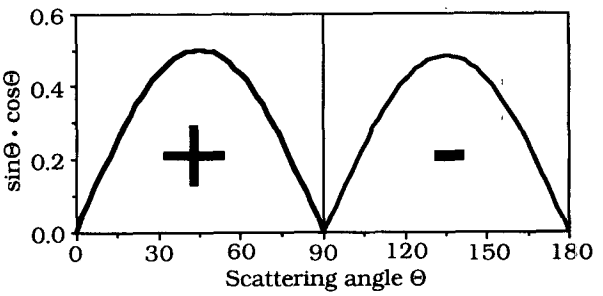

FIG. 6. Angular characteristics of a $\overline{\cos}\Theta$ nephelometer. The backscatter signal would be subtracted from the total scatter.

where B_x is the column burden of aerosol species x (i.e., $B_x = \int_0^\infty M_x(z)dz$, where z is altitude). The remaining variables [$f^\lambda(\mathrm{RH})$, β_0^λ and α_{sx}^λ] have been defined earlier in sections 9, 2, and 8, respectively, and are quantities or functions that can be totally or partially measured with the integrating nephelometer.

b. *Adaptations of the integrating nephelometer for determination of $f^\lambda(RH)$ related to climate forcing*

Two approaches have been developed for studies of $f^\lambda(\mathrm{RH})$, but most to date have not included measurement of its wavelength dependence. The earliest approach (as introduced in section 9) involved injection of water vapor in varying amounts into the inlet flow of the integrating nephelometer. Relative humidity was measured inside the chamber of the integrating nephelometer as the water vapor flux was increased continuously from zero to a maximum value (Charlson et al. 1974b). A second, reference integrating nephelometer kept at low RH by warming the flow or by addition of a known flow rate of desiccated, filtered air allowed the ratio of $\sigma_{sp}^\lambda(\mathrm{RH})/\sigma_{sp}^\lambda(\mathrm{RH_0})$ to be plotted as a continuous function of RH.

More recent versions of this system involve a humidistat as opposed to continuously varying the RH. One or more values of $\sigma_{sp}^\lambda(\mathrm{RH})$ at elevated RH is provided by passing the sample air flow through a tube that is permeable to water vapor but not liquid water (Covert and Heintzenberg 1993). The objective of measurements with this device is to obtain statistically meaningful amounts of data on $f^\lambda(\mathrm{RH})$ including its wavelength dependence for studies of both its variability and its dependence on other controlling variables such as the molecular composition of the aerosol, size distribution and particle morphology, state of mixing, etc.

c. *Adaptation of the integrating nephelometer for studies of the angular scattering function $f^\lambda(\Theta)$*

As introduced above in sections 2 and 10, the scattering function $f^\lambda(\Theta)$ comes into play in problems of radiative transfer because it describes the amount of radiant energy directed into different scattering angles Θ. For the problem of climate forcing by aerosols, it is necessary to know the relative amounts of light scattered upward toward space and downward toward the earth's surface. Only that which is directed upward can contribute to a direct climate forcing; light scattered toward the earth's surface is effectively the same as transmitted light in terms of heating, photosynthesis, etc.

While the specialized geometry of the asymmetry-parameter nephelometer has not yet been realized, a simpler instrument has been built that measures σ_{bsp}^λ by alternately inserting a shutter in front of the light source to eliminate light scattered from $\Theta \approx 0$ to $\Theta \approx \pi$, (cf. Fig. 2 in Charlson et al. 1974a). Heintzenberg and Bhardwaja (1976) studied the angular integration characteristics of this device, which has been analyzed further by Marshall (1994).

Bridging the gap between the ideal asymmetry parameter integrating nephelometer and the simple backscatter device, Marshall (1994) also produced calculated relationships of σ_{fsp}^λ to σ_{bsp}^λ, showing that a useful degree of correspondence is expected to exist for model calculations based on measured size distribution. However, there is not always a one-to-one dependence of σ_{fsp}^λ on σ_{bsp}^λ, depending on refractive index and size distributions.

d. *Studies of aerosol mass-scattering efficiency for the climate forcing problem*

Yet another approach is needed for determining α_{sx}^λ, namely, the simultaneous but separate determination of σ_{sp}^λ with the integrating nephelometer and M_x. Properly, sufficient numbers of simultaneous, collocated measurements would be made in order to yield a functional relationship of σ_{sp}^λ on M_x, which then is differentiated to yield $\alpha_{sx}^\lambda = \delta\sigma_{sp}^\lambda/\delta M_x$. This is often approximated by regression analysis of the dependence of σ_{sp}^λ on M_x (White 1986; Anderson et al. 1994). It is essential that the optical and mass/chemical determinations be made on the same size-resolved subset of the aerosol particles.

e. *Completing the set of input parameters for climate models: Wavelength dependence and single-scattering albedo*

While Eq. (11.1) was used in the earliest approximations of climate forcing—for example, by anthropogenic sulfate aerosol—and while the results of those studies indicated that such global-mean forcing was likely to be significant in magnitude and opposite in sign to forcing by greenhouse gases (Charlson et al. 1990; Charlson et al. 1991; Charlson et al. 1992), and while the variables in Eq. (11.1) probably do comprise the first-order controlling factors in calculating ΔF_R^λ, this simple formulation alone cannot provide a complete picture. On the one hand, solar radiation is not monochromatic and on the other, light absorption (e.g., by soot or black carbon) does occur, changing σ_{ep}^λ and adding a heating term to the equation.

Just as was the case with $f^\lambda(\Theta)$ and α_s^λ, it is possible to calculate the wavelength dependence of σ_{sp}^λ, often described by the Ångström exponent $\mathring{a}$ by using an assumed or measured size distribution, complex refractive index and particle shape (usually spherical). However, the multiwavelength integrating nephelometer designs after Ahlquist and Charlson (1969) makes possible the direct measurement of $\mathring{a}$ by measuring σ_{sp}^λ at two or more wavelengths and using finite-difference formulation to approximate a derivative. Since the Ångström exponent $\mathring{a}$ is defined by the relationship $\sigma_{sp}^\lambda \propto \lambda^{-\mathring{a}}$:

$$\mathring{a} = -\frac{d\log\sigma_{sp}^{\lambda}}{d\log\lambda}. \qquad (11.2)$$

Not only does this simple formulation make it possible to have a continuous quantitative output from the integrating nephelometer of $\mathring{a}$, it also makes possible a direct comparison to the traditional method of determining $\mathring{a}$ via multiwavelength solar photometry.

Measured light absorption by atmospheric aerosols can be used directly to calculate a heating rate within the atmosphere; however, it must be combined with α_s^{λ} in order to be used in Mie computations of scattering properties by particles with a finite amount of absorption as described by an imaginary refractive index of finite magnitude. While it usually has been necessary to assume the imaginary part of the refractive index or to estimate it from angular or other scattering studies, and then to perform Mie computation to yield both the absorption coefficient σ_{ap}^{λ} and σ_{sp}^{λ}, it is possible to directly measure σ_{ap}^{λ} and use it with σ_{sp}^{λ} measured with the integrating nephelometer to provide the input needed for the radiative transfer calculations. This obviates the need for any assumptions or Mie computations. Measurement of absorption, for example, with the integrating plate (Lin et al. 1973) or the integrating sphere (Heintzenberg 1982) methods can yield σ_{ap}^{λ}. This then is combined with σ_{sp}^{λ} to yield the single scattering albedo, ω^{λ}.

12. Conclusions

Having described the principles, evolution and applications of the integrating nephelometer, it is possible to summarize the applications and, most importantly, the fundamental design philosophy that permeates through all of them. The traditional way to describe aerosol optical properties in all problems of radiative transfer is to assume or measure size distribution, assume or measure complex refractive index and calculate all of the optical properties [σ_{sp}^{λ}, $\mathring{a}$, $f(\Theta)$, etc.] via the Mie (1908) formalism. Beuttell and Brewer (1949) not only designed an instrument, they established a design philosophy in which instruments are devised to directly measure the relevant integral aerosol parameters, thus eliminating the need for assumptions, complex calculations, and the unknown uncertainties associated with them. More to the point, this design philosophy allows two approaches to the determination of several parameters—direct measurement with the aid of the integrating nephelometer and calculation via the Mie formalism. Comparison of calculated and measured valued for a parameters allows *closure* studies—that is, the difference between them is an objective measure of the uncertainty that is inherent in the combined set of parameter values and the model. For example, Quinn et al. (1995) and Zhang et al. (1994) show disparities of less than 10% between measured σ_s and its value calculated from simultaneously measured size distributions. Anderson et al. (1996) show a similar degree of disparity between measured and calculated values of σ_s using laboratory generated, monodisperse aerosol. The result of this kind of exercise will be a clear definition and quantification of the uncertainties that exist in defining the optical properties of atmospheric aerosol.

REFERENCES

Ahlquist, N. C., and R. J. Charlson, 1967: A new instrument for measuring the visual quality of air. *J. Air Pollut. Control Assoc.*, **17,** 467–469.

——, and ——, 1969: Measurement of the wavelength dependence of atmospheric extinction due to scatter. *Atmos. Environ.*, **3,** 551–564.

Anderson, T. L., R. J. Charlson, W. H. White, and P. H. McMurry, 1994: Comment on "Light scattering and cloud condensation nucleus activity of sulfate aerosol measured over the Northeast Atlantic Ocean." *J. Geophys. Res.*, **99D,** 25 947–25 949.

——, and Coauthors, 1996: Performance characteristics of a high-sensitivity, three-wavelength, total scatter/backscatter nephelometer. *J. Atmos. Oceanic Technol.*, **13,** 967–986.

Ångström, A., 1929: On the atmospheric transmission of sun radiation and on dust in the air. *Geografiska Ann.*, **11,** 156–166.

Beuttell, R. G., and A. W. Brewer, 1949: Instruments for the measurement of the visual range. *J. Sci. Instrum.*, **26,** 357–359.

Bhardwaja, P. S., R. J. Charlson, A. P. Waggoner, and N. C. Ahlquist, 1973: Rayleigh scattering coefficients of Freon-12, Freon-22 and CO_2 relative to that of air. *Appl. Opt.*, **12,** 135.

——, J. Herbert, and R. J. Charlson, 1974: Refractive index of atmospheric particulate matter: an in situ method for determination. *Appl. Opt.*, **13,** 731–734.

——, J. Heintzenberg, and R. J. Charlson, 1976: Refractive index of atmospheric aerosols. *IAMAP Symp. on Radiation in the Atmosphere,* Garmisch Partenkirchen, Germany, IAMAP, 91–93.

Bodhaine, B. A., 1979: Measurement of the Rayleigh scattering properties of some gases with a nephelometer. *Appl. Opt.*, **18,** 121–125.

——, N. C. Ahlquist, and R. C. Schnell, 1991: Three-wavelength nephelometer suitable for aircraft measurement of background aerosol scattering coefficient. *Atmos. Environ.*, **25A,** 2267–2276.

Charlson, R. J., H. Horvath, and R. F. Pueschel, 1967: The direct measurement of atmospheric light scattering coefficient for studies of visibility and pollution. *Atmos. Environ.*, **1,** 469–478.

——, N. C. Ahlquist, and H. Horvath, 1968: On the generality of correlation of atmospheric aerosol mass concentration and light scatter. *Atmos. Environ.*, **2,** 455–464.

——, A. H. Vanderpol, D. S. Covert, A. P. Waggoner, and N. C. Ahlquist, 1974a: $H_2SO_4/(NH_4)_2SO_4$ background aerosol: Optical detection in St. Louis region. *Atmos. Environ.*, **8,** 1257–1267.

——, ——, ——, ——, and ——, 1974b: Sulfuric acid-ammonium sulfate aerosol: Optical detection in the St. Louis region. *Science,* **184,** 156–158.

——, W. M. Porch, A. P. Waggoner, and N. C. Ahlquist, 1974c: Background aerosol light scattering characteristics: Nephelometric observations at Mauna Loa Observatory compared with results at other remote locations. *Tellus,* **26,** 345–360.

——, D. S. Covert, T. V. Larson, and A. P. Waggoner, 1978: Chemical properties of tropospheric sulfur aerosols. *Atmos. Environ.*, **12,** 39–53.

——, ——, and ——, 1984: Observation of the effect of humidity on light scattering by aerosols. *Hygroscopic Aerosols,* L. H. Ruhnke and A. Deepak, Eds., 35–44.

——, J. Langner, and H. Rodhe, 1990: Sulphate aerosol and climate. *Nature,* **348,** 22.

——, ——, ——, C. B. Leovy, and S. G. Warren, 1991: Perturbation of the northern hemisphere radiative balance by backscattering of anthropogenic sulfate aerosols. *Tellus,* **43**(AB), 152–163.

——, S. E. Schwartz, J. M. Hales, R. D. Cess, J. A. Coakley Jr., J. E. Hansen, and D. J. Hofmann, 1992: Climate forcing by anthropogenic aerosols. *Science,* **256,** 423–430.

Covert, D. S., and J. Heintzenberg, 1993: Size distribution and chemical properties of aerosol at Ny-Ålesund, Svalbard. *Atmos. Environ.,* **27**(A), 2989–2997.

——, A. P. Waggoner, R. E. Weiss, N. C. Ahlquist, and R. J. Charlson, 1980: Atmospheric aerosols, humidity, and visibility. *The Character and Origins of Smog Aerosols,* G. M. Hidy, P. K. Mueller, D. Grosjean, B. R. Appel, and J. J. Wesolowski, Eds., Wiley & Sons, 559–581.

Crosby, P., and B. W. Koerber, 1963: Scattering of light in the lower atmosphere. *J. Opt. Soc. Amer.,* **53,** 358–361.

Cutten, D. R., 1974: Rayleigh scattering coefficients for dry air carbon dioxide and Freon-12. *Appl. Opt.,* **13,** 468–469.

Dzubay, T. G., R. K. Stevens, C. W. Lewis, D. H. Hern, W. J. Courtney, J. W. Tesch, and M. A. Mason, 1982: Visibility and aerosol composition in Houston, Texas. *Environ. Sci. Technol.,* **16,** 514–525.

Ensor, D. S., and A. P. Waggoner, 1970: Angular truncation error in the integrating nephelometer. *Atmos. Environ.,* **4,** 481–487.

Garland, J. A., and J. B. Rae, 1970: An integrating nephelometer for atmospheric studies and visibility warning devices. *J. Sci. Instrum.,* **3,** 275–280.

Gerber, H., 1986: Tethered balloon measurements at San Nicolas Island (Oct. 1984): Instrumentation, data summary, preliminary data interpretation. Naval Research Laboratory Rep. No. 8972, Washington, DC, 77 pp.

Hänel, G., 1976: The properties of atmospheric aerosol particles as functions of the relative humidity at thermodynamic equilibrium with the surrounding moist air. *Advances in Geophysics,* Vol. 16, Academic Press, 74–188.

Harrison, A. W., 1977: An automatic scanning integrating spectronephelometer. *Can. J. Phys.,* **55,** 1399–1406.

——, 1979: Nephelometer estimates of visual range. *Atmos. Environ.,* **13,** 645–652.

Hegg, D., T. Larson, and P.-F. Yuen, 1993: A theoretical study of the effect of relative humidity of light scattering by tropospheric aerosols. *J. Geophys. Res.,* **98,** 18 435–18 439.

Heinicke, J., 1967: Measurement of light scattering in the near infrared and visible spectral region with two scattered light recorders (in German). M.S. thesis, Dept. of Meteorology, University of Munich, 65 pp.

Heintzenberg, J., 1969: Extension of a visibility meter for the registration of spectral scattering coefficients in the visible and near infrared (in German). M.S. thesis, Dept. of Meteorology, University of Mainz, 70 pp.

——, 1975: Determination in situ of the size distribution of the atmospheric aerosol. *J. Aerosol Sci.,* **6,** 291–303.

——, 1977: Spectral light scattering and the atmospheric aerosol over the Atlantic. *'Meteor'-Forschungsergeb., Reihe B,* **12,** 1–9.

——, 1978: The angular calibration of the total scatter/backscatter nephelometer, consequences and applications. *Staub,* **38,** 62–63.

——, 1980: Particle size distribution and optical properties of Arctic haze. *Tellus,* **32,** 251–260.

——, 1982: Size-segregated measurements of particulate elemental carbon and aerosol light absorption at remote Arctic locations. *Atmos. Environ.,* **16,** 2461–2469.

——, 1985: What can we learn from aerosol measurements at baseline stations? *J. Atmos. Chem.,* **3,** 153–169.

——, and H. Quenzel, 1973a: Calculations on the determination of the scattering coefficient of turbid air with integrating nephelometers. *Atmos. Environ.,* **7,** 509–519.

——, and ——, 1973b: On the effect of the loss of large particles on the determination of scattering coefficients with integrating nephelometers. *Atmos. Environ.,* **7,** 503–507.

——, and P. S. Bhardwaja, 1976: On the accuracy of the backward hemispheric integrating nephelometer. *J. Appl. Meteor.,* **15,** 1092–1096.

——, and G. Witt, 1979: Extension of atmospheric light scattering measurements into the UV region. *Appl. Opt.,* **18,** 1281–1283.

——, and L. Bäcklin, 1983: A high sensitivity integrating nephelometer for airborne air pollution studies. *Atmos. Environ.,* **17,** 433–436.

——, J. Ström, J. A. Ogren, and H.-P. Fimpel, 1991: Vertical profiles of aerosol properties in the summer troposphere of the European Arctic. *Atmos. Environ.,* **25**(A), 621–628.

Horvath, H., and K. E. Noll, 1969: The relationship between atmospheric light scattering coefficient and visibility. *Atmos. Environ.,* **3,** 543–550.

Husar, R. B., K. T. Whitby, and B. Y. H. Liu, 1972: Physical mechanisms governing the dynamics of Los Angeles smog aerosol. *J. Colloid Interface Sci.,* **39,** 211.

Jones, M. R., K. H. Leong, M. Q. Brewster, and B. P. Curry, 1994: Inversion of light scattering measurements for particle size and optical constants: Experimental study. *Appl. Opt.,* **33,** 4035–4041.

Junge, C., 1952: *Gesetzmäßigkeiten in der Größenverteilung atmosphärischer Aerosole über dem Kontinent.* Rep. 35, Deutscher Wetterdienst in der US-Zone, 261–277.

Kasten, F., 1968: Rayleigh-Cabannes-Streuung in trockener Luft unter Berücksichtigung neuerer Depolarisations-Messungen. *Optik,* **27,** 155–166.

Koschmieder, H., 1924: Theorie der horizontalen Sichtweite. *Contrib. Atmos. Phys.,* **43,** 33–55.

Lin, C.-I., M. Baker, and R. J. Charlson, 1973: Absorption coefficient of atmospheric aerosol: A method for measurement. *Appl. Opt.,* **12,** 1356–1363.

Marshall, S. F., 1994: Measurement-derived radiative transfer parameters for the aerosol climate forcing problem. M.S. thesis, Dept. of Atmospheric Sciences, University of Washington, 112 pp.

Mathai, C. V., and A. W. Harrison, 1980: Estimation of atmospheric aerosol refractive index. *Atmos. Environ.,* **14,** 1131–1135.

Mie, G., 1908: Beiträge zur Optik trüber Medien, speziell kolloidaler Metallösungen. *Ann. Phys.,* **25,** 377–445.

Nyeki, S. A. P., I. Colbeck, and R. M. Harrison, 1992: A portable aerosol sampler to measure real-time atmospheric mass loadings. *J. Aerosol Sci.,* **23** (Suppl. 1), S687–S690.

Pilat, J., and R. J. Charlson, 1966: Theoretical and optical studies of humidity effects on the size distribution of a hygroscopic aerosol. *J. Rech. Atmos.,* **1,** 165–170.

Quenzel, H., 1969: Der Einfluss der Aerosolgrößenverteilung auf die Messgenauigkeit von Streulichtmessern. *Gerlands Beitr. Geophys.,* **78,** 251–263.

——, G. H. Ruppersberg, R. Schellhase, and J. Heintzenberg, 1974: Berechnungen des systematischen Fehlers von Streulichtmeßgeräten. *Second Conf. of the Gesellschaft für Aerosolforschung (GAeF),* Bad Soden, Germany, GAeF, 96–101.

——, ——, and ——, 1975: Calculations about the systematic error of visibility—Meters measuring scattered light. *Atmos. Environ.,* **9,** 587–601.

Quinn, P. K., S. F. Marshall, T. S. Bates, D. S. Covert, and V. N. Kapustin, 1995: Comparison of measured and calculated aerosol properties relevant to the direct radiative forcing of tropospheric sulfate aerosol on climate. *J. Geophys. Res.,* **100**(D5), 8977–8991.

Rabinoff, R. A., and B. M. Herman, 1973: Effect of aerosol size distribution on the accuracy of the integrating nephelometer. *J. Appl. Meteor.,* **12,** 184–186.

Radke, L. F., and P. V. Hobbs, 1969: An automatic cloud condensation nuclei counter. *J. Appl. Meteor.,* **8,** 105–109.

Rood, M. J., T. V. Larson, D. S. Covert, and N. C. Ahlquist, 1985: Measurement of laboratory and ambient aerosols with temperature and humidity controlled nephelometry. *Atmos. Environ.,* **19,** 1181–1190.

——, D. S. Covert, and T. V. Larson, 1987a: Hygroscopic properties of atmospheric aerosol in Riverside, California. *Tellus,* **39**(B), 383–397.

——, ——, and ——, 1987b: Temperature and humidity controlled nephelometry: improvements and calibration. *Aerosol Sci. Technol.,* **7,** 57–656.

Ruppersberg, G. H., 1959: *Recent approaches to recording the visibility on airports.* Scientific Society for Air Traffic, 230–236.

——, 1964: Registrierung der Sichtweite mit dem Streulichtschreiber. *Contrib. Atmos. Phys.*, **37,** 252–263.

——, 1978: The correct spectral weighting of the meteorological visibility. *Contrib. Atmos. Phys.*, **51,** 247–256.

——, H. V. Redwitz, and R. Schellhase, 1975: Atmospheric transmission and scattering in the visible and in the windows of the IR-region to 5 μm (in German). Rep. No. T 752-I-203.

Sagan, C., and J. B. Pollack, 1967: Anisotropic nonconservative scattering and the clouds of Venus. *J. Geophys. Res.*, **72,** 469–477.

Sverdrup, G. M., and K. T. Whitby, 1977: Determination of submicron atmospheric aerosol size distributions by use of continuous analog sensors. *Environ. Sci. Technol.*, **11,** 1171–1176.

Trijonis, J. C., W. C. Malm, M. Pitchford, W. H. White, R. Charlson, and R. Husar, 1990: Visibility: Existing and historical conditions—Causes and effects. Rep. No. 24, 24–85.

van de Hulst, H. C., 1957: *Light Scattering by Small Particles.* Wiley & Sons, 470 pp.

Vanderpol, A. H., F. D. Carsey, D. S. Covert, R. J. Charlson, and A. P. Waggoner, 1975: Aerosol chemical parameters and air mass character in the St. Louis region. *Science,* **190,** 570.

Waldram, J. M., 1945: Measurement of the photometric properties of the upper atmosphere. *Trans. Illum. Eng. Soc.*, **10,** 147–188.

Weiss, R., A. P. Waggoner, R. J. Charlson, and N. C. Ahlquist, 1977: Sulfate aerosol: Its geographical extent in the midwestern and southern United States. *Science,* **195,** 979–981.

White, W. H., 1986: On the theoretical and empirical basis for apportioning extinction by aerosols: A critical review. *Atmos. Environ.*, **20,** 1659–1672.

Winkler, P., 1973: The growth of atmospheric aerosol particles as a function of the relative humidity. Part II: An improved concept of mixed nuclei. *J. Aerosol Sci.*, **4,** 373–387.

——, J. Heintzenberg, and D. Covert, 1981: Vergleich zweier Messverfahren zur Bestimmung der Quellung von Aerosolpartikeln mit der relativen Feuchte. *Meteor. Rundsch.*, **34,** 114–119.

Wiscombe, W. J., and G. W. Grams, 1976: The backscattered fraction in two-stream approximations. *J. Atmos. Sci.*, **33,** 2440–2451.

Zhang, X., B. J. Turpin, P. H. McMurry, S. V. Hering, and M. R. Stolzenburg, 1994: Mie theory evaluation of species contributions to 1990 wintertime visibility reduction in the Grand Canyon. *J. Air Waste Manage. Assoc.*, **44,** 153–162.